

# Combining HFEPR and NMR Spectroscopies to Characterize Organochromium(III) Complexes with Large Zero-Field Splitting

J. Krzystek,<sup>†</sup> Gerald Kohl,<sup>‡</sup> Helge-Boj Hansen,<sup>‡</sup> Markus Enders,<sup>\*,‡</sup> and Joshua Telser<sup>\*,§</sup>

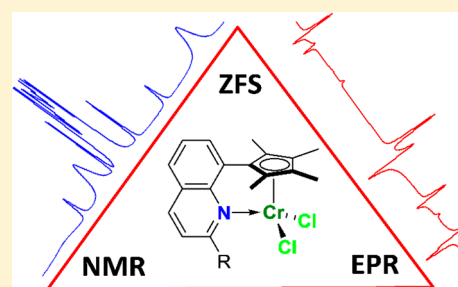
<sup>†</sup>National High Magnetic Field Laboratory, Florida State University, Tallahassee, Florida 32310, United States

<sup>‡</sup>Institute of Inorganic Chemistry, Heidelberg University, Im Neuenheimer Feld 270, 69120 Heidelberg, Germany

<sup>§</sup>Department of Biological, Physical and Health Sciences, Roosevelt University, 430 S. Michigan Avenue, Chicago, Illinois 60605, United States

## Supporting Information

**ABSTRACT:** A series of three organochromium(III) complexes, based on a quinoline-substituted cyclopentadienyl ring coordinated to a CrCl<sub>2</sub> moiety—C<sub>5</sub>Me<sub>4</sub>(C<sub>9</sub>NH<sub>6</sub>)CrCl<sub>2</sub> (**1**), C<sub>3</sub>Ph<sub>4</sub>(C<sub>9</sub>NH<sub>6</sub>)CrCl<sub>2</sub> (**2**), and C<sub>3</sub>Me<sub>4</sub>(C<sub>11</sub>NH<sub>10</sub>)CrCl<sub>2</sub> (**3**)—has been investigated by EPR spectroscopy, including high-frequency and -field EPR (HFEPR) as well as by <sup>1</sup>H NMR. Complex **3** is new and has higher solubility than **1** and **2**, which could potentially improve its activity as an alkene polymerization precatalyst, an application that has already been documented for **1** and **2**. The HFEPR studies show that **1–3** exhibit zero-field splitting (zfs) that is unusually large for Cr(III) (3d<sup>3</sup>, *S* = 3/2), as given by the axial zfs parameter *D* ≥ ~3 cm<sup>-1</sup>. The zfs determined here for **1** is in good agreement with previous theoretical studies of this complex by other workers, which were made in the absence of any knowledge of the experimental data. Such a “blind” comparison of theory and experiment is very rare. The NMR spectra of **3** are fully analyzed using the zfs data and clearly show the dominant contribution of Fermi contact shifts, now that the pseudocontact (dipolar) shifts can be accurately determined. The results show the power of integrated magnetic resonance (EPR and NMR) spectroscopy combined with theoretical calculations in understanding the subtleties of electronic structure of the paramagnetic organometallic complex, in this case with *S* > 1/2, which could then be related to chemical reactivity or magnetic properties.



## INTRODUCTION

The interplay between magnetically active (*I* ≠ 0) atomic nuclei and unpaired electrons (*S* ≠ 0) manifests itself in paramagnetic resonance techniques whether the electron(s), as in EPR, or the nuclei, as in NMR, are directly interrogated. Unpaired electrons influence significantly the magnetic properties of practically all NMR active nuclei in a molecule, leading to dramatic changes in relaxation behavior and chemical shift. Due to an inverse proportionality between line widths in EPR and NMR, highly resolved spectra can usually be obtained in only one or the other of these two magnetic resonance techniques. An intermediate case in terms of EPR and NMR line widths is chromium(III) complexes with cyclopentadienyl (Cp) ligands.<sup>1–3</sup> Such compounds are relevant for catalytic olefin polymerization processes.<sup>4–9</sup> Calculations have shown that the spin state and several agostic interactions during the reaction pathway play a crucial role for the low barrier of alkene insertion and the resulting high turnover numbers.<sup>10–12</sup> Consequently, experimentally determined parameters help to understand the electronic structure of such compounds and may lead to a better knowledge of the factors determining catalytic activity and selectivity. In addition to that aspect, a good correlation between theory and experiment for compounds, which can be isolated and characterized by independent methods (i.e., X-ray diffraction of **1** and **2**), will

pave the way for EPR/NMR spectroscopic identification of reaction intermediates during catalytic reactions.

EPR as well as NMR investigations CrCp<sub>*n*</sub> (*n* = 2 or 1, with ancillary ligands) species were published several years ago but were recently complemented by a comprehensive theoretical study on a range of cyclopentadienyl complexes, including Cr<sup>II</sup>Cp<sub>2</sub> and a Cr<sup>III</sup>Cp complex to be described below.<sup>13,14</sup>

The main contribution to the NMR chemical shift in such compounds is the Fermi-contact shift (fcs), which correlates with delocalization of unpaired electron density onto all measured NMR nuclei. Therefore, spin-density distribution in the whole molecule can easily be determined by NMR, whereas EPR fails to give a complete spin-density distribution as most hyperfine splittings are not resolved. On the other hand, EPR and, in particular, high-frequency and -field EPR (HFEPR) techniques<sup>15,16</sup> are well suited to obtain data such as *g*-anisotropy or zero-field splitting. Anisotropy in the *g* values can be present in any system with unpaired electrons and can be substantial in, e.g., low-spin d<sup>5</sup> complexes.<sup>17,18</sup> Zero-field splitting (zfs), however, is manifest only in systems with multiple unpaired electrons (*S* ≥ 1).<sup>19,20</sup> Such anisotropic magnetic effects also influence the NMR spectra to some

Received: March 10, 2019

Published: April 29, 2019

extent. Nevertheless, an integrated magnetic resonance approach that combines EPR and NMR spectroscopic measurements on the same system(s) is relatively uncommon. Exceptions worth noting, one of low-spin, the other of high-spin systems, are the separate studies by Clarke and co-workers<sup>21</sup> and by Franco and co-workers<sup>22</sup> on Ru(III) and/or Os(III) (4,5d<sup>5</sup>,  $S = 1/2$ ) penta- and/or tetraammine complexes and by Tierney and co-workers on Co(II) (3d<sup>7</sup>,  $S = 3/2$ ) hydridotrispyrazolylborate (Tp, “scorpionate”) complexes.<sup>23,24</sup>

Due to the lack of EPR data, effects of  $g$  anisotropy and zero-field splitting could be only roughly estimated in our earlier work on NMR spectroscopy of organochromium compounds.<sup>25</sup> Inspired by the above-mentioned integrated paramagnetic resonance studies on later transition metal ions (groups 8 and 9), we now present a similar approach to an early transition metal system, namely, Cr(III) (3d<sup>3</sup>,  $S = 3/2$ ). Specifically, HFEPR measurements of three derivatives of donor functionalized cyclopentadienyl chromium(III) complexes are described, and the influence of  $g$  anisotropy and zero-field splitting on the interpretation of the NMR spectroscopic data is explored. Additionally, our experimental results fully validate the previous theoretical study that included one of our complexes.<sup>14</sup>

## EXPERIMENTAL SECTION

Complexes **1** and **2** were synthesized according to published procedures.<sup>8,26</sup>

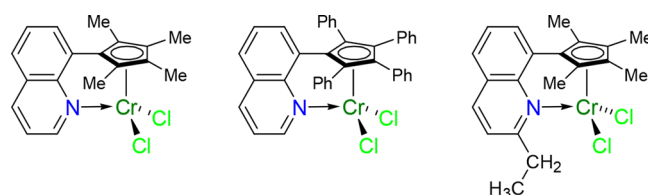
**Synthesis of 3.** 8-Bromo-2-ethylquinoline was synthesized by dropwise addition of 17.66 g of *trans*-2-pentenal (0.21 mol) to a refluxing mixture of 34.4 g (0.2 mol) of 2-bromoaniline in 50 mL of concentrated hydrochloric acid. After 60 min under reflux, the mixture was cooled to room temperature, and 27.2 g of ZnCl<sub>2</sub> (0.2 mol) was added. This mixture was then cooled to 0 °C, and 250 mL of acetone was added leading to a brown precipitate. The latter was collected and subsequently washed with 3 M HCl (aq), isopropanol, and diethyl ether. The remaining solid was treated with 50 mL of ammonia and extracted with diethyl ether. The organic solution was concentrated under a vacuum and distilled (0.012 mbar, 100 °C), leading to 14.8 g (55 mmol, 27.8% yield) of 8-bromo-2-ethylquinoline.

An amount of 10 g (42 mmol) of 8-bromo-2-ethylquinoline in 200 mL of tetrahydrofuran was cooled to −90 °C and lithiated with 18.6 mL (46.6 mmol) of *n*-butyllithium (2.5 M in hexanes). To this solution, 7.26 g (52.5 mmol) of tetramethylcyclopentenone was added at the same temperature. The mixture was allowed to warm to room temperature and was then heated to reflux for 1 h. After cooling to room temperature, 50 g of ice and 10 mL of aqueous HCl were added (pH < 1). After stirring overnight, the solution was treated with aqueous NH<sub>3</sub> (pH > 10). The organic phase was separated, and the aqueous phase was extracted three times with 50 mL of pentane. Distillation at 130–140 °C (0.03 mbar) gives 7.32 g (26.4 mmol, 62%) of the crude protio-ligand as a mixture of three isomers, which can be further purified by column chromatography. An amount of 554 mg (2.0 mmol) of the protio-ligand (isomeric mixture) in 30 mL of THF was deprotonated with 84 mg (2.1 mmol) of KH at room temperature within 2 h. The resulting dark red suspension was added to 712 mg (1.9 mmol) of CrCl<sub>3</sub>·3THF<sup>27</sup> in 30 mL of THF. After stirring overnight, the solvent was removed in a vacuum, and the solid was extracted with CH<sub>2</sub>Cl<sub>2</sub>. After removal of the solvent in a vacuum, the solid was washed with hexane and recrystallized from CH<sub>2</sub>Cl<sub>2</sub> to obtain 490 mg (1.23 mmol, 64%) of complex **3**. Elemental Analysis calcd.: C 60.16, H: 5.55, N: 3.51. Found: C 60.61, H 5.60, N: 3.60.

**(HFEPR Spectroscopy.** X-band (~9.5 GHz) EPR spectra of **3** (see Scheme 1) in dichloromethane solution were recorded using a Bruker Elexsys E500 EPR Spectrometer.

HFEPR experiments were performed in the spectrometer using a 15 T superconducting magnet, described earlier<sup>28</sup> with the exception of employing a Virginia Diodes (Charlottesville, VA, USA) source

## Scheme 1. Chromium Complexes Studied in This Work, Left to Right: 1, 2, and 3



operating at a base frequency of 12–14 GHz and multiplied by a cascade of multipliers. Phase-sensitive detection was used, with the magnetic field modulated at 50 kHz, so that traditional, first-derivative mode spectra resulted. Temperature control was provided by an Oxford Instruments (Oxford, UK) continuous flow cryostat. For HFEPR, complexes **1–3**, shown in Scheme 1, were loaded into 1 mL polyethylene vial containers in a glovebag under nitrogen either as ground powders or as toluene/dichloromethane (1:1 v/v) solutions, using dry, degassed solvents. The amount of solid material was 20–30 mg. In solution experiments, typically a similar amount (~20 mg) was dissolved in ~1 mL of solvent of which ~300 μL was transferred to the HFEPR sample vial.

The spin Hamiltonian parameters were obtained by least-squares fits to field vs frequency maps of the turning points in the powder spectra<sup>15</sup> using the program SPIN (by A. Ozarowski), which employs a standard spin Hamiltonian for spin quartets:<sup>29</sup>

$$H = \mu_B B \cdot g \cdot \hat{S} + D \left( \hat{S}_z^2 - \frac{1}{3} S(S+1) \right) + E (\hat{S}_x^2 - \hat{S}_y^2) \quad (1)$$

The same program served to simulate single-frequency spectra.

**NMR Spectroscopy.** Proton NMR spectra of **1–3** were recorded in CDCl<sub>3</sub> solution at room temperature with a Bruker DRX200 spectrometer. Typically, 4000 transients were recorded with a 90° pulse length of 13.3 μs and a repetition time of 65 ms.

## RESULTS AND DISCUSSION

Three organochromium(III) complexes sketched in Scheme 1 were chosen for this study. Compounds **1** and **2** have been reported previously and were used as precatalysts in ethylene polymerization.<sup>8,26</sup> Compound **3** is a newly synthesized derivative which features much higher solubility compared to **1** and **2**, simply by virtue of the ethyl substituent at position 2 of the quinoline ring.

**Conventional (X-band) EPR.** The X-band EPR spectrum of **3** in frozen dichloromethane solution is shown in Figure 1. Such a spectrum is typical of a system with  $S = 3/2$ , wherein the microwave quantum energy (here,  $\nu = 9.60$  GHz,  $0.32$  cm<sup>−1</sup>) is much smaller than the zfs, which in the case of a rhombic, spin quartet system ( $E$  term in eq 1 is nonzero) is often denoted as  $\Delta$ , and is given by<sup>20</sup>

$$\Delta = 2\sqrt{D^2 + 3E^2} \quad (2)$$

For small  $E$  values, as is the case here,  $\Delta \approx 2D$ . The other information obtained from the X-band spectrum is that the sign of  $D$  (with the sign of  $E$  conventionally taken to be the same) is positive. In this case, the  $\langle S, M_S | = \langle 3/2, \pm 1/2 |$  Kramers doublet is lower in energy (ground spin state) and the  $\langle 3/2, \pm 3/2 |$  Kramers doublet is higher in energy (excited spin state). Such a situation yields a perpendicular feature at  $g_{\perp} \approx 4$  and a parallel feature at  $g_{\parallel} \approx 2$ , as seen in Figure 1. If the sign of  $D$  were negative, then the X-band EPR spectral appearance would be dramatically different, as seen for Co(II) complexes,<sup>23</sup> especially for organocobalt(II) at a low coordination number.<sup>30–32</sup>

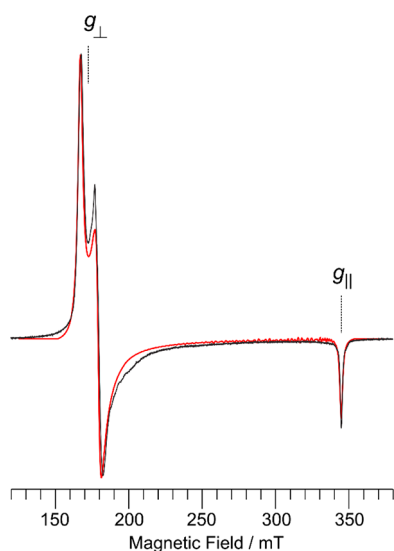


**Figure 1.** X-band EPR spectrum of **3** in dichloromethane solution recorded at 4.8 K and 9.60 GHz (black trace) with simulation (red trace). The simulation uses an effective spin,  $S' = 1/2$ , with  $g' = [4.10, 3.88, 1.988]$  and with Lorentzian line widths (hwhm) of 110, 118, and 32 MHz. The feature labeled  $g_{\perp}$  is split into  $g'_{\max}$  (lower field) and  $g'_{\text{mid}}$  (higher field) features due to rhombic zfs.

The simulation shown in Figure 1 employs an effective  $S' = 1/2$  to yield effective  $g'$  values (here only in order  $g'_{\max}$ ,  $g'_{\text{mid}}$ ,  $g'_{\min}$ ): 4.10, 3.88, and 1.988. Use of a perturbation theory equation<sup>20</sup> with  $E/D = 0.02$  and intrinsic (i.e., “true”  $S = 3/2$  spin Hamiltonian), isotropic  $g$  values of 1.99 yields effective  $g'$  values as follows:  $g'_x = 3.86$ ,  $g'_y = 4.10$ , and  $g'_z = 1.988$ , in good agreement with the experiment.

**HFEPR.** Complex **1** measured as a solid produced fairly strong but broad and ill-defined EPR resonances at low temperature (10 K) that could only be partly interpreted retroactively once an experiment on frozen solution was performed. Figure S1 (Supporting Information) shows a typical solid spectrum accompanied by simulations using  $S = 3/2$  spin Hamiltonian parameters obtained from a glass.

Given the poor quality of the spectra obtained from the solid **1**, we prepared a solution in a mix of toluene and dichloromethane (~1:1 v/v). The obtained low-temperature glass spectra were of much higher quality, although with a lower signal-to-noise ratio due to the absorption of the sub-THz wave radiation by the glass. In particular, the line widths of the observed turning points were much narrower than in the

solid and their shape much better defined and consistent with a powder pattern. Figure S2 (Supporting Information) shows a typical HFEPR spectrum of the glass under the same conditions as in Figure S1. The appearance of the near-zero field resonance at this frequency yields an immediate estimate of  $2|D| \sim 203 \text{ GHz} = 6.77 \text{ cm}^{-1}$ , i.e.,  $|D| \sim 3.38 \text{ cm}^{-1}$ . Simulations of this spectrum use more accurate spin Hamiltonian parameters for  $S = 3/2$ , obtained using the tunable-frequency methodology (see Figure S3, Supporting Information),<sup>15</sup> listed in Table 1. A comparison of the experiment with simulations shows that the zero-field splitting parameter  $D$  is positive, in agreement with the X-band spectrum for the similar complex, **3**.

Compound **2** as a solid produced very high-quality spectra at any temperature from liquid helium to ambient. The spectra were consistent with a powder distribution of the crystallites in the sample and were characterized by a much smaller line width than in the case of complex **1**. Figure 2 shows a typical

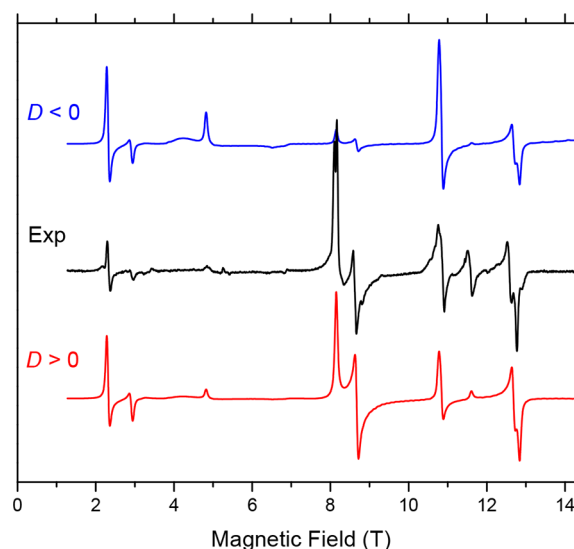


**Figure 2.** EPR spectrum of solid **2** at 7 K and 321.6 GHz (black trace) accompanied by simulations (colored traces) using spin Hamiltonian parameters as listed in Table 1 in the case of both negative and positive  $D$ . The resonance at ca. 11.6 T ( $g = 1.98$ ) originates from an unknown isotropic Cr species and is not simulated.

spectrum at a low temperature (7 K) of the solid, together with its simulations using spin Hamiltonian parameters as in Table 1, again for the case of both negative and positive  $D$ . The

**Table 1.** Spin Hamiltonian Parameters for the Three Complexes Studied

compound	temp. (K)	$D$ ( $\text{cm}^{-1}$ )	$E$ ( $\text{cm}^{-1}$ )	$E/D$	$g_x$	$g_y$	$g_z$	$g_{\text{iso}}$
<b>1</b> <sup>a</sup>	10	+3.29(1)	+0.046(1)	0.014	1.980(2)	1.976(4)	2.02(4) <sup>d</sup>	1.99
<b>1</b> (theory) <sup>b</sup>	298	+2.8 – + 3.0	+0.09 – + 0.14	0.032–0.047	1.952–1.965	1.944–1.959	1.979–1.985	1.958–1.970
<b>2</b> <sup>c</sup>	7	+3.126(5)	+0.087(3)	0.028	1.981(3)	1.975(2)	1.982(6)	1.979
<b>2</b> <sup>c</sup>	280	+3.14(1)	+0.085(6)	0.027	1.977(6)	1.980(2)	1.98 <sup>e</sup>	1.98
<b>3</b> <sup>a,c</sup>	5–10	+3.25(1)	+0.120(7)	0.037	1.967(5)	1.962(6)	1.970(8)	1.966

<sup>a</sup>Data in frozen toluene/dichloromethane 1:1 v/v solution. <sup>b</sup>Values calculated by Rouf et al. (see their Table 4).<sup>14</sup> We present here the range of values calculated by four different levels of theory; see text for further discussion. The calculated  $g$  values are matched with the most closely corresponding experimental values, so that  $g_{\max} \equiv g_z$ ,  $g_{\text{mid}} \equiv g_y$ , and  $g_{\min} \equiv g_x$ . Their NMR values (see Table S1) were calculated at 298 K, so we assume the same applies for the spin Hamiltonian parameters. <sup>c</sup>Data in the solid state. For complex **3**, the parameters in the solution are identical to those in solid, although they were not determined via the tunable-frequency methodology so the errors do not apply to the solution data. <sup>d</sup>The large error in  $g_z$  is due to a limited number of observable parallel turning points. <sup>e</sup> $g_z$  needed to be constrained to a value of 1.98 in the fits because of the same problem as in *d*.

parameters were obtained using the tunable-frequency methodology, see Figure 3. The magnitude of the zfs

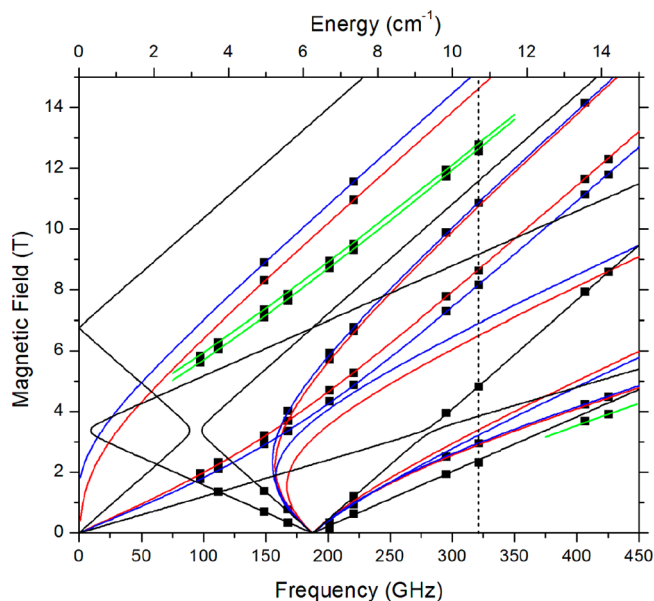


**Figure 3.** Magnetic field vs frequency (or energy) dependence of the turning points in HFEPR spectra of solid **2** observed at 7 K. Squares are experimental points; curves were drawn using best-fitted spin Hamiltonian parameters as in Table 1. Red curves: turning points with the magnetic field  $B_0$  parallel to the  $x$ -axis of the zfs tensor. Blue curves,  $B_0 \parallel y$ ; black curves,  $B_0 \parallel z$ ; green curves, off-axis turning points. The dashed vertical line represents the frequency at which the spectrum shown in Figure 2 was recorded.

parameters is similar to those of **1** as measured in solution, with the rhombicity factor about twice as much but still very small, and  $D$  remains positive as indicated by the similarity of the observed spectra with those simulated using  $D > 0$ . Further proof of the sign of  $D$  was delivered by following the temperature dependence of the spectra as shown in Figure S5 and explained in Figure S6 (both in the Supporting Information).

Sample **2** produced HFEPR spectra up to room temperature. Figure 4 shows a spectrum at 280 K and 321.6 GHz together with its simulation using spin Hamiltonian parameters as in Table 1 while Figure S4 (Supporting Information) presents the field vs frequency map in the same conditions. At room temperature, the ground and excited Kramers doublets are essentially equally populated, so there is no spectral dependence on the sign of  $D$ ; only the case of positive  $D$  is simulated. The magnitude of the zfs parameters is slightly larger at room temperature than at 10 K. We did not perform an experiment on **2** in solution due to its low solubility.

Solid complex **3** displayed spectra that were almost as good as those of **2** (Figure S7, Supporting Information). The spin Hamiltonian parameters are very similar to those of **1**, with  $D$  being almost identical, while  $E$  is three times as large as in **1** (and 50% larger than in **2**). For the actual values, obtained through the tunable-frequency methodology (Figure S8, Supporting Information), see Table 1. The resonances could be pursued up to 80 K and beyond, but no room temperature spectra were recorded. Complex **3** in solution produced resonances that were identical in position to those of the solid,

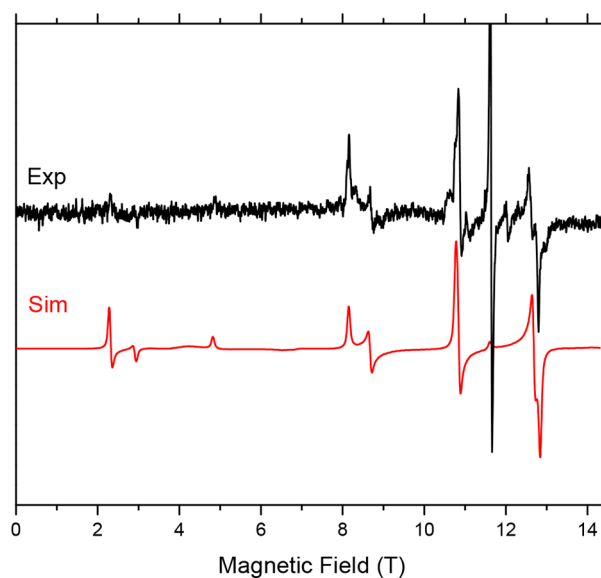


**Figure 4.** EPR spectrum of solid **2** at 280 K and 321.6 GHz (black trace) accompanied by a simulation (red trace) using spin Hamiltonian parameters as listed in Table 1. The resonance at ca. 11.6 T ( $g = 1.98$ ) originates from an unknown isotropic Cr species and is not simulated.

but with decreased S/N ratio due to sub-THz wave power losses by solvent absorption (Figure 5).

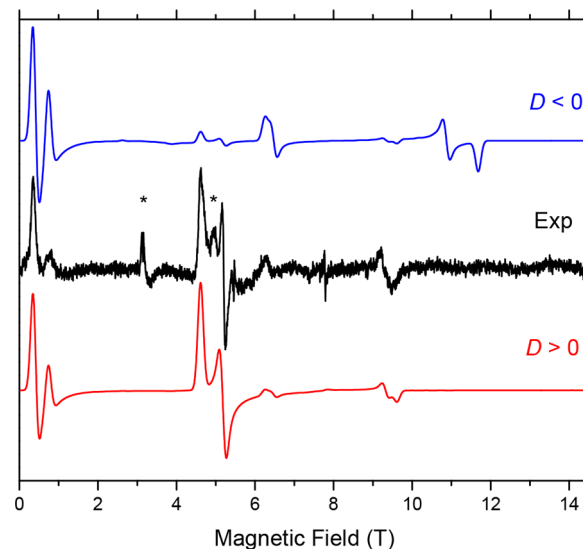


**Figure 5.** EPR spectrum of **3** in toluene/dichloromethane 1:1 v/v solution at 10 K and 216 GHz (black trace) accompanied by simulations (colored traces) using spin Hamiltonian parameters as listed in Table 1 in the case of both negative, and positive  $D$ . The resonances in the experimental spectrum marked with asterisks originate from solid molecular dioxygen and are not simulated. Neither is the peak at ca. 7.77 T ( $g = 1.98$ ) that originates from an unknown isotropic Cr species.

### Comparison with previous EPR theoretical results.

Quantum chemical theory (QCT) has been widely applied in recent years toward understanding the electronic structure of paramagnetic transition metal complexes.<sup>33–36</sup> Typically, the computational/theoretical studies are undertaken after the experimental data are reported. An example is the HFEPR

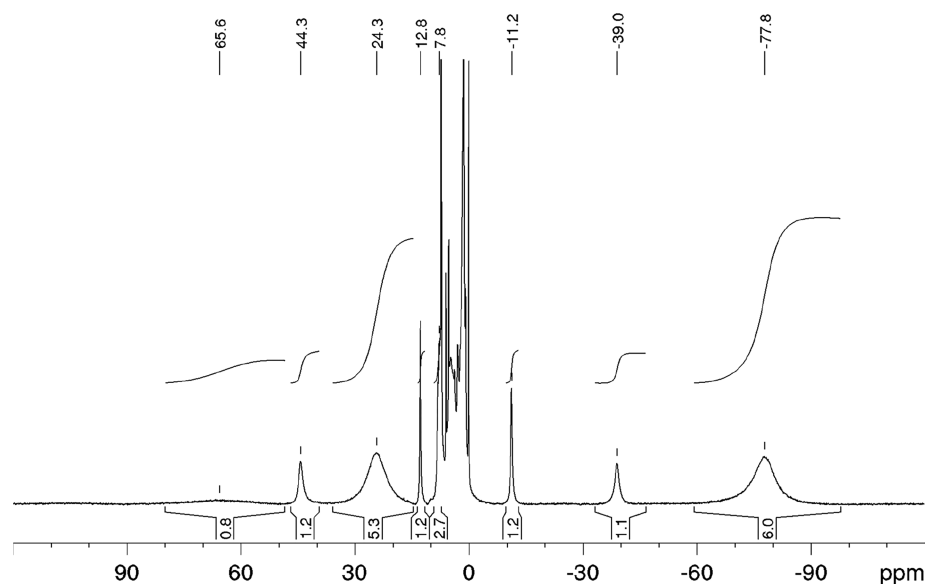


**Figure 6.**  $^1\text{H}$  NMR spectrum of **3** in  $\text{CDCl}_3$  measured at 295 K and 200 MHz.

study of Ni(II) ( $3d^8$ ,  $S = 1$ ) scorpionate complexes of general formula  $\text{TpNiX}$  ( $X = \text{Cl, Br, I}$ ),<sup>37</sup> which was followed by a detailed computational study that explained the trend in zfs as a function of the halido ligand.<sup>38</sup> Alternatively, the experimental and theoretical studies are performed in concert, as was the case with another Ni(II) scorpionate, which was coordinated by a  $\kappa^3$ -hydridoborato ligand.<sup>39</sup> The situation that pertains here is highly unusual in that the computational studies<sup>13,14</sup> were performed *before* there were any experimental data. The earlier computational study by Vaara and co-workers included  $\text{MCp}_2$  ( $M = \text{Cr and Ni}$ ) as well as **1**, and the later, more comprehensive one focused on neutral, paramagnetic metallocene complexes of general formula  $\text{MCp}_2$  ( $M = \text{V, Cr, Mn, Co, Rh, Ir, and Ni}$ ), but also included **1**.<sup>14</sup> We speculate that **1** was included because the authors were unaware of any simple  $[\text{Cr}^{\text{III}}\text{Cp}_2]^+$  species, although such a chromocenium complex was reported many years ago,<sup>40</sup> but absent any spectroscopic or structural characterization. In any case, Vaara and co-workers calculated the zfs and  $g$  values for **1** in their later paper,<sup>14</sup> and these results are also presented in Table 1. The authors used four different levels of theory: CASSCF and NEVPT2 calculations, each of which used either the def2-TZVP basis set with nonrelativistic (NR + SO) wave functions or the DKH-TZV basis set with relativistic (DKH + SO) wave functions. The relative merits of each method are beyond the scope of our work, but it is clear that all of these methods, as evidenced by the narrow range of calculated values (see Table 1), give excellent correspondence with the experiment. The CASSCF (NR + SO) method gave an ever so slightly higher  $D$  value ( $3.0 \text{ cm}^{-1}$ ) compared to both NEVPT2 methods ( $2.8 \text{ cm}^{-1}$ ), but this hardly demonstrates any superiority of this approach. Both CASSCF methods gave slightly higher rhombicity than both NEVPT2 methods ( $E/D = 0.046$  (0.047) versus 0.032). These values are all slightly higher than the experiment, but the rhombicity is a difficult parameter to determine computationally. Likewise for the  $g$  values, wherein the  $g$  anisotropy, and hence the deviation from  $g_{\text{e}}$ , appears to be overstated by the theory, with the NEVPT2 methods giving slightly less anisotropy/deviation and thus modestly better agreement with the experiment. One cannot

generalize as to whether the relativistic (DKH) or non-relativistic (NR) approach is superior, although we suspect, as nonexperts, that for a  $3d$  ion such as Cr(III), relativistic methods are not critically needed, in contrast to a  $5d$  ion.<sup>41</sup> Nevertheless, the overall agreement between the calculated and experimental spin Hamiltonian parameters for **1** is remarkable, especially given that Vaara and co-workers had no prior knowledge of the experimental data.

There are a number of Cr(III) coordination complexes for which the zfs has been determined but in most cases are six-coordinate, slightly distorted or truly octahedral complexes, wherein the relatively high symmetry causes the zfs to be of small magnitude. Trigonal distorted examples are  $\text{Cr}(\text{acac})_3$ , for which  $D \approx 0.6 \text{ cm}^{-1}$ ,<sup>42,43</sup> and a trigonal Cr(III) complex even with heteroleptic coordination (N3C3 donor set) exhibits similar zfs:  $D = 0.45 \text{ cm}^{-1}$  for  $(\text{iPrtacn})\text{Cr}(\text{CN})_3$  ( $\text{iPrtacn} = 1,4,7$ -tris-isopropyl-1,4,7-triazacyclononane).<sup>44</sup> A classic, early X-band EPR study was on an extensive series of complexes of general formula  $\text{trans}[\text{CrL}_4\text{XY}]^{n+}$  ( $L = \text{NH}_3, \text{py}$ ;  $X, Y = \text{halide, H}_2\text{O, etc.}$ ), which yielded a range of  $D$  values ( $\sim 0 < |D| \leq \sim 0.7 \text{ cm}^{-1}$ ), but with  $|D| \approx 0.2 \text{ cm}^{-1}$  being typical.<sup>45</sup> W-band (94.5 GHz) EPR of a tetragonally distorted Cr(III) complex,  $\text{trans-RSSR}[\text{CrCl}_2(\text{cyclam})]^+$  ( $\text{cyclam} = 1,4,8,11$ -tetraazacyclotetradecane), provided  $D \approx -0.3 \text{ cm}^{-1}$ .<sup>46,47</sup> Tetragonal Cr(III) complexes with chelating diphosphine ligands have been explored for use as single molecule (single ion) magnets.<sup>48</sup> These octahedral complexes of general formula  $[\text{Cr}(\text{dmpe})_2(\text{CN})\text{X}]^+$  ( $X = \text{Cl, Br, I}$ ;  $\text{dmpe} = 1,2$ -bis-(dimethylphosphino)ethane) exhibit a wide range of zfs:  $0.11 \leq |D| \leq 2.3 \text{ cm}^{-1}$ .<sup>48</sup> However, in this series the magnitude of  $D$  increases with halido ligand size and is highest with iodido ligand (similarly with the Cr(II) congeners), which is the result of spin-orbit coupling (SOC) involving this heavy atom. The heavy atom effect on zfs has been shown in a number of cases, such as the  $\text{TpNiX}$  series,<sup>38</sup> Co(II) complexes,<sup>49</sup> and a Mn(III) coordination complex,<sup>50</sup> and has been fully described in systematic experimental/computational studies by Duboc and co-workers on Mn(II)<sup>51</sup> and Mn(III)<sup>52</sup> complexes.

Thus, it is difficult to put the spin Hamiltonian results, whether experimental or theoretical, for **1**–**3** into context of

other such systems as there are no direct Cr(III) analogs, except to note that the magnitude of  $D$  seen here, which is absent any heavy atom ligand effects, is quite large for a Cr(III) complex. Vanadocene is another neutral metallocene complex with a  $3d^3$  ion, V(II), albeit with much higher symmetry than 1–3. Also notable is that the free-ion SOC constant of  $V^{2+}$  is nearly 40% smaller than that of  $Cr^{3+}$  ( $\zeta = 169$  versus  $274 \text{ cm}^{-1}$ ),<sup>53</sup> which would thus reduce the zfs for directly analogous systems.<sup>19,20</sup> However, EPR studies of this complex<sup>54–56</sup> provided  $D = +2.836(2) \text{ cm}^{-1}$  ( $E = 0$  for this axial species),<sup>55</sup> which is nearly as large as that seen for 1–3. Vaara and co-workers calculated  $D = +2.4(1) \text{ cm}^{-1}$ , the range given here ( $\pm 0.1 \text{ cm}^{-1}$ ) arising from the different computational methods they employed. This calculated value is  $\sim 15\%$  lower than the experiment one and that for 1 is roughly  $\sim 12\%$  lower, information which may be of use for advances in “benchmarking” theory.

**NMR Spectroscopy.** All three compounds are able to adopt  $C_s$  symmetry in solution, and therefore pairs of substituents at the five-membered rings become equivalent in NMR spectra. The  $^1\text{H}$  NMR spectrum of 3 is shown in Figure 6. Two large signals with a relative intensity of 6.0 and 5.3 can be attributed to the four  $\text{CH}_3$  substituents at the Cp ring. Two of the five quinoline H atoms resonate at high field ( $-39.0$  and  $-11.2$  ppm, respectively) and two at low field ( $44.3$  and  $12.8$  ppm, respectively), whereas a fifth signal is hidden in the diamagnetic region (i.e., from 8 to 0 ppm). The solvent signal ( $7.2$  ppm) shows a large shoulder at  $\sim 7$ – $8$  ppm which integrates to 2.7 and is assigned to the  $\text{CH}_3$  group of the ethyl substituent. The corresponding  $\text{CH}_2$  signal is very broad (width at half height =  $2500 \text{ Hz}$ ) and located at  $65.6$  ppm. This extreme line broadening is due the close proximity of these H atoms to the chromium center, and therefore a fast relaxation results. The fast relaxation associated with the very broad line leads to a small intensity of this signal (only 0.8 instead of 2.0).

In order to assign the NMR signals in a better way, we have to discuss and apply the theory which describes the influence of unpaired electrons on NMR spectra. Several effects contribute to the chemical shift and relaxation behavior of NMR nuclei, which still makes it difficult to interpret NMR spectra of paramagnetic molecules. Only if a single contribution dominates, then the NMR analysis becomes straightforward.<sup>57–61</sup> In a simplified approach, three main contributions add up to the observed chemical shift ( $\delta_{\text{exp}}$ ), namely, the orbital shift ( $\delta_{\text{orb}}$ ), which is also present in diamagnetic systems, the Fermi-contact shift (fcs) and the pseudocontact shift (pcs). The first contribution ( $\delta_{\text{orb}}$ ) is usually known from isostructural diamagnetic compounds or can be calculated with high precision by increment systems or by DFT. The fcs contribution is proportional to the unpaired spin-density at the measured nucleus, whereas pcs comes from a dipolar electron–nucleus interaction and is proportional to the magnetic anisotropy of the molecule.

The main paramagnetic shift contribution for the complexes studied in this work is fcs which itself correlates with the spin density at the measured nucleus according to eq 3 ( $\mu_0$  is the vacuum permeability,  $\mu_B$  the Bohr magneton,  $g_e$  the free electron  $g$  factor,  $k$  the Boltzmann factor,  $S$  the total spin quantum number,  $T$  the temperature, and  $\rho_{\alpha\beta}$  the spin density at the measured nucleus):

$$\text{fcs} = \frac{\mu_0 \mu_B^2 g_e^2}{9k} \times \frac{(S+1)}{T} \rho_{\alpha\beta} \quad (3)$$

Spin density can be calculated by DFT methods. Figure 7 shows the correlation of the calculated with the experimental

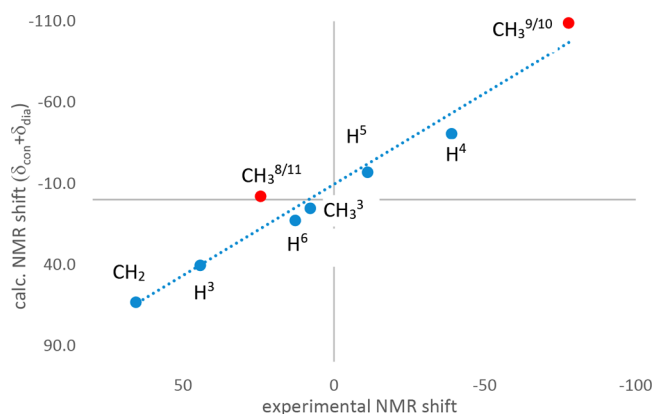


**Figure 7.** Correlation of experimental NMR shift of 3 measured at 295 K with the sum of the calculated fcs and the diamagnetic shift. The red dots lie somewhat outside the linear correlation and are assigned to the  $\text{CH}_3$  groups at the Cp ring.

NMR shifts. The calculated shifts used eq 3 with the addition of the orbital shift (i.e., diamagnetic shift). The calculation of the spin density nicely correlates with the experimental paramagnetic shifts with the exception of the two resonances of the  $\text{CH}_3$  substituents at the Cp rings.

The correlation between spin density and experimental paramagnetic shift demonstrates that the paramagnetic shift is dominated by fcs and that pcs is small. However, with the help of the EPR results, we can now estimate the small contribution from pcs, which is itself a result of magnetic anisotropy. The main source of magnetic anisotropy is located at the metal center so that a point dipole model is appropriate for the description of pcs (see eq 4,  $\Delta\chi_{\text{ax}}$  and  $\Delta\chi_{\text{rh}}$  are the axial and rhombic components of the magnetic susceptibility tensor,  $\theta$  and  $\varphi$  are angles between the metal–NMR nucleus vector and the axes defining the magnetic anisotropy, and  $r$  is the distance between the metal and NMR nucleus.)

$$\text{pcs} = \frac{1}{4\pi} \left[ \frac{1}{3} \Delta\chi_{\text{ax}} \times \frac{3 \cos^2 \theta - 1}{r^3} + \frac{1}{2} \Delta\chi_{\text{rh}} \times \frac{\sin^2 \theta \cos 2\varphi}{r^3} \right] \quad (4)$$

Metal centered magnetic anisotropy ( $\Delta\chi$ ) stems from  $g$  anisotropy and zfs. If the size and sign of these parameters are known, then  $\Delta\chi$  can be calculated. Consequently, the position of a resonating NMR nucleus (parameters  $r$ ,  $\theta$ , and  $\varphi$ ) together with  $g$  anisotropy and zfs define the pseudocontact shift. The relation between pcs,  $g$  anisotropy, and zfs has been described by Kurland and McGarvey.<sup>62</sup> In the absence of significant rhombic magnetic anisotropy, pcs can be described as the sum of a contribution from  $g$  anisotropy (pcs<sup>g</sup>) and zfs (pcs<sup>zfs</sup>) with

$$\text{pcs}^g = \frac{\mu_0}{4\pi} \times \frac{\mu_B^2 S(S+1)}{9kT} \times \frac{3 \cos^2 \theta - 1}{r^3} \times (g_{\parallel}^2 - g_{\perp}^2) \quad (5a)$$

Table 2. Results of Calculations of pcs Contributions  $pcs^g$  and  $pcs^{zfs}$  using eqs 5a and 5b, respectively, for 3<sup>a</sup>

	$r$ [Å]	Cr–N axis			Cr–Cp axis				
		$\theta$ (Cr–N)	$pcs^g$	$pcs^{zfs}$	$pcs$	$\theta$ (Cr–Cp)	$pcs^g$	$pcs^{zfs}$	$pcs$
H <sup>3</sup>	5.338	19.9	0.23	−0.7	−0.47	131.57	0.04	−0.14	−0.09
H <sup>4</sup>	6.087	4.26	0.18	−0.57	−0.39	107.65	−0.07	0.21	0.14
H <sup>5</sup>	6.463	26.9	0.11	−0.33	−0.22	84.79	−0.08	0.23	0.16
H <sup>6</sup>	6.461	49	0.02	−0.07	−0.05	62.69	−0.03	0.09	0.06
H <sup>7</sup>	4.863	68.5	−0.11	0.34	0.23	43.16	0.11	−0.34	−0.23
CH <sub>3</sub> <sup>8/11</sup>	3.55–4.34	133.2–161.5	−0.35	1.1	0.75	46.6–68.9	−0.13	0.39	0.26
CH <sub>3</sub> <sup>9/10</sup>	3.55–4.34	133.2–161.5	0.35	−1.1	−0.75	43.8–65.6	−0.07	0.22	0.15
CH <sub>2</sub> <sup>12</sup>	2.83/4.26	47.1/60.8	−0.08	0.25	0.17	155.8/172.3	1.09	−3.41	−2.32
CH <sub>3</sub> <sup>13</sup>	4.16–5.27	21.6–62.9	0	−0.02	−0.02	142.6–162.0	0.23	−0.72	−0.49

<sup>a</sup>An axial model has been used with  $g_{\parallel} = g_z$ ,  $g_{\perp} = 0.5(g_x + g_y)$ , and  $E = 0$ . Left side: axis along Cr–N vector (blue dotted line in Figure 8). Right side: axis along Cp–centroid–Cr vector (red dotted line in Figure 8). H numbering is shown in Figure 8.

$$\begin{aligned}
 pcs^{zfs} = & -\frac{\mu_0}{4\pi} \times \frac{\mu_B^2 S(S+1)(2S-1)(2S+1)}{135k^2 T^2} \\
 & \times \frac{3 \cos^2 \theta - 1}{r^3} \times \left( g_{\parallel}^2 - \frac{1}{2} g_{\perp}^2 \right) \times D_z \quad (5b)
 \end{aligned}$$

The contribution from  $g$  anisotropy has a  $T^{-1}$  dependence, whereas the contribution from  $zfs$  has a  $T^{-2}$  dependence. The HFEPR data show a positive  $g$  anisotropy ( $= g_{\parallel} - g_{\perp}$ ) and a positive  $D$  so that the two contributions to the  $pcs$  have opposite sign and they cancel to some extent.

Table 2 lists the contributions of both  $g$  anisotropy and  $zfs$  to  $pcs$  for all H nuclei in compound 3, with the H numbering scheme given in Figure 8. Two orientations of the magnetic

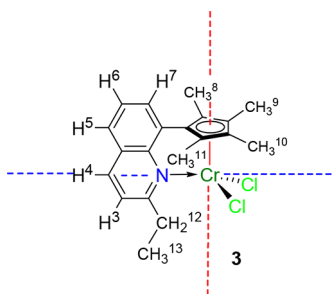


Figure 8. H numbering scheme for compound 3. The red dotted line shows one possible axis in an axial model as used for the analysis of  $pcs$  (i.e., the axis defined by the Cr–Cp centroid vector), whereas the blue dotted line shows the other possibility (i.e., defined by the Cr–N(quinoline) vector).

axis have been used: along the Cr–N bond and along the line connecting the Cr atom with the centroid of the Cp ring. In both orientations,  $pcs$  values are quite small with a maximum value of  $-2.3$  ppm only. These values are too small to affect the  $^1\text{H}$  NMR spectrum of 3 (see Figures 6 and 7). The axial component of the magnetic anisotropy tensor ( $\Delta\chi_{\text{ax}}$ ) was calculated from the  $pcs$  values by using the axial part of eq 4 leading to a small magnetic anisotropy of  $1.7 \times 10^{-33} \text{ m}^3$ . For comparison,  $\Delta\chi_{\text{ax}}$  values in Co(II) or Fe(II) typically lie in the range of  $8 \times 10^{-32}$  to  $4 \times 10^{-31} \text{ m}^3$ .<sup>63–65</sup> This small magnetic anisotropy value clearly shows that  $pcs$  is very small so that  $fcs$  is the dominating paramagnetic shift contribution in 1–3 and related compounds.

**Comparison with Previous NMR Theoretical Results.** The calculated and experimental chemical shifts for 1 and 3 are given in Table S1 (Supporting Information). Such data for 1

have already been presented by Vaara and co-workers<sup>14</sup> but are given here for convenience and to highlight both the experimental differences between 1 and 3 and the differences between experiment and theory for 1.

## SUMMARY

HFEPR has been successfully applied to a series of organochromium(III) complexes that are relevant as precatalysts for alkene polymerization.<sup>8,25,26</sup> These complexes exhibit a spin quartet, i.e.,  $S = 3/2$ , ground state, which is typical for Cr(III), but the spin Hamiltonian parameters extracted by HFEPR show that the  $zfs$  is unusually large in magnitude for these complexes. Generally, coordination complexes of Cr(III) are six-coordinate with distorted octahedral geometry and exhibit relative modest  $zfs$ , with the axial  $zfs$  parameter,  $|D| < 0.5 \text{ cm}^{-1}$ , absent any complicating factors, such as from heavy atom ligands.<sup>48,50</sup> In contrast, complexes 1–3 exhibit  $D > 3 \text{ cm}^{-1}$ , which is as large in magnitude as any mononuclear Cr(III) complex of which we are aware. Interestingly, the  $zfs$  for isoelectronic V(II) in vanadocene is nearly as large ( $D = 2.8 \text{ cm}^{-1}$ ).<sup>55</sup>

The determination by HFEPR of the  $zfs$  in the previously unreported complex 3 now allows a complete theoretical analysis of the paramagnetic shifts in its  $^1\text{H}$  NMR, complex 1 having been previously analyzed in this way using calculated  $zfs$  parameters,<sup>14</sup> which we now show are quite close to experimental results. These calculations show that despite the significant magnetic anisotropy of these Cr(III) centers, the pseudocontact shift ( $pcs$ ) is still relatively small so that the Fermi-contact shift ( $fcs$ ) is the dominant source of the chemical shifts in the  $^1\text{H}$  NMR of these complexes. The results of this study show in general the applicability of an integrated magnetic resonance approach to paramagnetic organometallic complexes. Such an approach can be used to distinguish subtle differences among a series of related complexes that could then be correlated with chemical reactivity or magnetic properties. In addition to that potential application, the excellent agreement between the theoretically predicted and experimentally determined values may help to identify reaction intermediates in catalytic reactions by EPR/NMR techniques.

## ASSOCIATED CONTENT

### Supporting Information

The Supporting Information is available free of charge on the ACS Publications website at DOI: 10.1021/acs.organomet.9b00158.

Additional HFEPR spectra, energy-level, and 2D field-frequency diagrams (Figures S1–S8); table of experimental and calculated NMR chemical shifts (PDF)

## AUTHOR INFORMATION

### Corresponding Authors

\*E-mail: markus.enders@uni-heidelberg.de.

\*E-mail: jtelsler@roosevelt.edu.

### ORCID

J. Krzystek: 0000-0001-6088-1936

Markus Enders: 0000-0003-0415-1992

Joshua Telser: 0000-0003-3307-2556

### Notes

The authors declare no competing financial interest.

## ACKNOWLEDGMENTS

The authors acknowledge support by the state of Baden-Württemberg through bwHPC and the German Research Foundation (DFG) through grant no INST 40/467-1 FUGG. A portion of this work was performed at the National High Magnetic Field Laboratory, which is supported by the United States National Science Foundation through Cooperative Agreements No. DMR-1157490 and DMR-1644779 and by the State of Florida. We thank Dr. Andrew Ozarowski (NHMFL) for his EPR fit and simulation software SPIN. We also thank Dr. Ozarowski and Dr. Samuel M. Greer (NHMFL) for assistance with some of the HFEPR experiments.

## REFERENCES

- (1) Köhler, F. H. KMR-spektroskopie an paramagnetischen komplexen: XI.  $^{13}\text{C}$ -,  $^1\text{H}$ -spektren und darstellung alkylierter nickelocene, kobaltocene, chromocene und vanadocene. *J. Organomet. Chem.* **1976**, *110*, 235–246.
- (2) Grohmann, A.; Köhler, F. H.; Müller, G.; Zeh, H. Dialkyl( $\eta^5$ -cyclopentadienyl)chromium Derivatives with Extreme Values of  $^{12}\text{H}$ -NMR Parameters. *Chem. Ber.* **1989**, *122*, 897–899.
- (3) Hebenanz, N.; Köhler, F. H.; Scherbaum, F.; Schlesinger, B. NMR spectroscopy of paramagnetic complexes. Part 36— $^{2/1}\text{H}$  NMR of paramagnetic metallocenes: Primary and secondary isotope effects and signal narrowing. *Magn. Reson. Chem.* **1989**, *27*, 798–802.
- (4) Thomas, B. J.; Theopold, K. H. Cationic chromium(III) alkyls as olefin polymerization catalysts. *J. Am. Chem. Soc.* **1988**, *110*, 5902–5903.
- (5) Theopold, K. H. Homogeneous Chromium Catalysts for Olefin Polymerization. *Eur. J. Inorg. Chem.* **1998**, *1998*, 15–24.
- (6) Döhrring, A.; Göhre, J.; Jolly, P. W.; Kryger, B.; Rust, J.; Verhovnik, G. P. J. Donor-Ligand-Substituted Cyclopentadienylchromium(III) Complexes: A New Class of Alkene Polymerization Catalyst. 1. Amino-Substituted Systems. *Organometallics* **2000**, *19*, 388–402.
- (7) Jones, D. J.; Gibson, V. C.; Green, S. M.; Maddox, P. J.; White, A. J. P.; Williams, D. J. Discovery and Optimization of New Chromium Catalysts for Ethylene Oligomerization and Polymerization Aided by High-Throughput Screening. *J. Am. Chem. Soc.* **2005**, *127*, 11037–11046.
- (8) Enders, M.; Fernández, P.; Ludwig, G.; Pritzkow, H. New chromium(III) complexes as highly active catalysts for olefin polymerization. *Organometallics* **2001**, *20*, 5005–5007.
- (9) Sturzel, M.; Mihan, S.; Mulhaupt, R. From Multisite Polymerization Catalysis to Sustainable Materials and All-Polyolefin Composites. *Chem. Rev.* **2016**, *116*, 1398–433.
- (10) Jensen, V. R.; Angermund, K.; Jolly, P. W.; Børve, K. J. Activity of Homogeneous Chromium(III)-Based Alkene Polymerization

Catalysts: Lack of Importance of the Barrier to Ethylene Insertion. *Organometallics* **2000**, *19*, 403–410.

(11) Döhrring, A.; Jensen, V. R.; Jolly, P. W.; Thiel, W.; Weber, J. C. Donor-Ligand-Substituted Cyclopentadienylchromium(III) Complexes: A New Class of Alkene Polymerization Catalyst. 2. Phosphinoalkyl-Substituted Systems. *Organometallics* **2001**, *20*, 2234–2245.

(12) Xu, R.; Klatt, G.; Enders, M.; Köppel, H. Theoretical Evaluation of Ethylene Insertion into Chromium Alkyl Bonds of Cp-Donor-Based Olefin Polymerization Catalysts. *J. Phys. Chem. A* **2012**, *116*, 1077–1085.

(13) Vaara, J.; Rouf, S. A.; Mareš, J. Magnetic Couplings in the Chemical Shift of Paramagnetic NMR. *J. Chem. Theory Comput.* **2015**, *11*, 4840–4849.

(14) Rouf, S. A.; Mareš, J.; Vaara, J. Relativistic Approximations to Paramagnetic NMR Chemical Shift and Shielding Anisotropy in Transition Metal Systems. *J. Chem. Theory Comput.* **2017**, *13*, 3731–3745.

(15) Krzystek, J.; Zvyagin, S. A.; Ozarowski, A.; Trofimenko, S.; Telser, J. Tunable-frequency high-field electron paramagnetic resonance. *J. Magn. Reson.* **2006**, *178*, 174–183.

(16) Telser, J.; Krzystek, J.; Ozarowski, A. High-frequency and high-field electron paramagnetic resonance (HFEPR): a new spectroscopic tool for bioinorganic chemistry. *JBIC, J. Biol. Inorg. Chem.* **2014**, *19*, 297–318.

(17) McGarvey, B. R. Survey of ligand field parameters of strong field  $d^5$  complexes obtained from the g matrix. *Coord. Chem. Rev.* **1998**, *170*, 75–92.

(18) Rieger, P. H. Electron paramagnetic resonance studies of low-spin  $d^5$  transition metal complexes. *Coord. Chem. Rev.* **1994**, *135*–136, 203–286.

(19) Boča, R. Zero-field splitting in metal complexes. *Coord. Chem. Rev.* **2004**, *248*, 757–815.

(20) Telser, J. EPR Interactions - Zero-Field Splittings. In *eMagRes*; John Wiley & Sons, Ltd, 2017; Vol. 6, pp 207–233.

(21) LaChance-Galang, K. J.; Doan, P.; Clarke, M. J.; Rao, U.; Yamano, A.; Hoffman, B. M. EPR and NMR Spectra as Probes of Spin-Density Distributions in Heterocyclic Ligands Coordinated in *trans*-[L(Im)(NH<sub>3</sub>)<sub>4</sub>Ru<sup>III</sup>]: Crystal Structure of *trans*-[(Im)<sub>2</sub>(NH<sub>3</sub>)<sub>4</sub>Ru]Cl<sub>2</sub>·H<sub>2</sub>O. *J. Am. Chem. Soc.* **1995**, *117*, 3529–3538.

(22) McGarvey, B. R.; Batista, N. C.; Bezerra, C. W. B.; Schultz, M. S.; Franco, D. W.  $^1\text{H}$  NMR and EPR Studies of [M(NH<sub>3</sub>)<sub>5</sub>(H<sub>2</sub>O)]-(TFMS)<sub>3</sub> (M = Ru, Os). Theory of the Paramagnetic Shift for Strong Field  $d^5$  Complexes. *Inorg. Chem.* **1998**, *37*, 2865–2872.

(23) Myers, W. K.; Duesler, E. N.; Tierney, D. L. Integrated paramagnetic resonance of high-spin Co(II) in axial symmetry: Chemical separation of dipolar and contact electron-nuclear couplings. *Inorg. Chem.* **2008**, *47*, 6701–6710.

(24) Myers, W. K.; Scholes, C. P.; Tierney, D. L. Anisotropic Fermi Couplings Due to Large Unquenched Orbital Angular Momentum: Q-Band  $^1\text{H}$ ,  $^{14}\text{N}$ , and  $^{11}\text{B}$  ENDOR of Bis(trispyrazolylborate) Cobalt(II). *J. Am. Chem. Soc.* **2009**, *131*, 10421–10429.

(25) Fernández, P.; Pritzkow, H.; Carbó, J. J.; Hofmann, P.; Enders, M.  $^1\text{H}$  NMR Investigation of Paramagnetic Chromium(III) Olefin Polymerization Catalysts: Experimental Results, Shift Assignment and Prediction by Quantum Chemical Calculations. *Organometallics* **2007**, *26*, 4402–4412.

(26) Ronellenfisch, M.; Gehrman, T.; Wadepohl, H.; Enders, M. Improving 1-Hexene Incorporation of Highly Active Cp-Chromium-Based Ethylene Polymerization Catalysts. *Macromolecules* **2017**, *50*, 35–43.

(27) Jones, P. J.; Hale, A. L.; Levason, W.; McCullough, F. P. Synthesis and properties of tetrahydrofuran complexes of chromium(III). [Cr(THF)<sub>3</sub>X<sub>3</sub>] (X = Cl, Br, I), [Cr(THF)<sub>2</sub>X<sub>4</sub>]<sup>−</sup> (X = Cl, Br, I, NCS), and [Cr(THF)<sub>6</sub>](BF<sub>4</sub>)<sub>3</sub>. *Inorg. Chem.* **1983**, *22*, 2642–2644.

(28) Hassan, A. K.; Pardi, L. A.; Krzystek, J.; Sienkiewicz, A.; Goy, P.; Rohrer, M.; Brunel, L.-C. Ultrawide band multifrequency high-field EMR technique: a methodology for increasing spectroscopic information. *J. Magn. Reson.* **2000**, *142*, 300–312.

- (29) Weil, J. A.; Bolton, J. R. *Electron Paramagnetic Resonance: Elementary Theory and Practical Applications*, 2nd ed.; John Wiley & Sons, Inc.: Hoboken, NJ, 2007.
- (30) Ding, K.; Dugan, T. R.; Brennessel, W. W.; Bill, E.; Holland, P. L. Synthesis, Properties, and Reactivity of Diketiminato-Supported Cobalt Fluoride Complexes. *Organometallics* **2009**, *28*, 6650–6656.
- (31) Przyojski, J. A.; Arman, H. D.; Tonzetich, Z. J. NHC Complexes of Cobalt(II) Relevant to Catalytic C-C Coupling Reactions. *Organometallics* **2013**, *32*, 723–732.
- (32) Massard, A.; Braunstein, P.; Danopoulos, A. A.; Choua, S.; Rabu, P. Studies on Three-Coordinate  $[\text{Co}\{\text{N}(\text{SiMe}_3)_2\}_2\text{L}]$  Complexes, L = N-Heterocyclic Carbene. *Organometallics* **2015**, *34*, 2429–2438.
- (33) Neese, F. Prediction of molecular properties and molecular spectroscopy with density functional theory: From fundamental theory to exchange-coupling. *Coord. Chem. Rev.* **2009**, *253*, 526–563.
- (34) Neese, F.; Pantazis, D. A. What is not required to make a single molecule magnet. *Faraday Discuss.* **2011**, *148*, 229–238.
- (35) Atanasov, M.; Ganyushin, D.; Sivalingam, K.; Neese, F. A Modern First-Principles View on Ligand Field Theory Through the Eyes of Correlated Multireference Wavefunctions. In *Molecular Electronic Structures of Transition Metal Complexes II*; Mingos, D. M. P.; Day, P.; Dahl, J. P., Eds.; Springer: Berlin, 2012; pp 149–220.
- (36) Neese, F. First Principles Approach to Spin-Hamiltonian Parameters. In *Multifrequency Electron Paramagnetic Resonance*; Misra, S. K., Ed.; Wiley-VCH Verlag GmbH & Co. KGaA: Weinheim, Germany, 2011; pp 295–326.
- (37) Desrochers, P. J.; Telser, J.; Zvyagin, S. A.; Ozarowski, A.; Krzystek, J.; Vivic, D. A. Electronic Structure of Four-Coordinate  $\text{C}_{3v}$  Nickel(II) Scorpionate Complexes: Investigation by High-Frequency and -Field Electron Paramagnetic Resonance and Electronic Absorption Spectroscopies. *Inorg. Chem.* **2006**, *45*, 8930–8941.
- (38) Ye, S.; Neese, F. How Do Heavier Halide Ligands Affect the Signs and Magnitudes of the Zero-Field Splittings in Halogenonickel(II) Scorpionate Complexes? A Theoretical Investigation Coupled to Ligand-Field Analysis. *J. Chem. Theory Comput.* **2012**, *8*, 2344–2351.
- (39) Desrochers, P. J.; Sutton, C. A.; Abrams, M. L.; Ye, S.; Neese, F.; Telser, J.; Ozarowski, A.; Krzystek, J. Electronic Structure of Nickel(II) and Zinc(II) Borohydrides from Spectroscopic Measurements and Computational Modeling. *Inorg. Chem.* **2012**, *51*, 2793–2805.
- (40) Fischer, E. O.; Ulm, K.; Kuzel, P. Über Aromaten-Komplexe von Metallen. LXVI. Über Cyclopentadienyl-Halogen-Komplexe des Chroms. *Z. Anorg. Allg. Chem.* **1963**, *319*, 253–265.
- (41) Pyykkö, P. The Physics behind Chemistry and the Periodic Table. *Chem. Rev.* **2012**, *112*, 371–384.
- (42) Elbers, G.; Remme, S.; Lehmann, G. EPR of chromium(3+) in tris(acetylacetonato)gallium(III) single crystals. *Inorg. Chem.* **1986**, *25*, 896–897.
- (43) The  $g$  factors were determined to high precision in this doped single-crystal study, but the value given here is a consensus for several different diamagnetic hosts.
- (44) Rebilly, J.-N.; Catala, L.; Charron, G.; Rogez, G.; Rivière, E.; Guillot, R.; Thuéry, P.; Barra, A.-L.; Mallah, T. Magnetic anisotropy of two trinuclear and tetranuclear  $\text{Cr}^{\text{III}}\text{Ni}^{\text{II}}$  cyanide-bridged complexes with spin ground states  $S = 4$  and  $S = 5$ . *Dalton Trans.* **2006**, 2818–2828.
- (45) Pedersen, E.; Toftlund, H. Electron spin resonance spectra of tetragonal chromium(III) complexes. I. *trans*- $[\text{Cr}(\text{NH}_3)_4\text{XY}]^{n+}$  and *trans*- $\text{Cr}(\text{py})_4\text{XY}^{n+}$  in frozen solutions and powders. Correlation between zero-field splittings and ligand field parameters via complete d-electron calculations. *Inorg. Chem.* **1974**, *13*, 1603–1612.
- (46) Solano-Peralta, A.; Sosa-Torres, M. E.; Flores-Alamo, M.; El-Mkami, H.; Smith, G. M.; Toscano, R. A.; Nakamura, T. High-field EPR study and crystal and molecular structure of *trans*  $\text{R}[\text{CrCl}_2(\text{cyclam})]_n\text{X}$  (X =  $\text{ZnCl}_4^{2-}$ ,  $\text{Cl}^-$  and  $\text{Cl}^- \cdot 4\text{H}_2\text{O} \cdot 0.5\text{HCl}$ ). *Dalton Trans.* **2004**, 2444–2449.
- (47) The  $g$  factors were determined to high precision in this relatively high-frequency and -field study, but the value given here is a consensus for complexes with different counteranions and with spectra recorded at 10 K versus ambient temperature.
- (48) Karunadasa, H. I.; Arquero, K. D.; Berben, L. A.; Long, J. R. Enhancing the Magnetic Anisotropy of Cyano-Ligated Chromium(II) and Chromium(III) Complexes via Heavy Halide Ligand Effects. *Inorg. Chem.* **2010**, *49*, 4738–4740.
- (49) Saber, M. R.; Dunbar, K. R. Ligand effects on the magnetic anisotropy of tetrahedral cobalt complexes. *Chem. Commun.* **2014**, *50*, 12266–12269.
- (50) Mossin, S.; Weihe, H.; Barra, A.-L. Is the Axial Zero-Field Splitting Parameter of Tetragonally Elongated High-Spin Manganese(III) Complexes Always Negative? *J. Am. Chem. Soc.* **2002**, *124*, 8764–8765.
- (51) Duboc, C.; Phoeung, T.; Zein, S.; Pécaut, J.; Collomb, M.-N.; Neese, F. Origin of the Zero-Field Splitting in Mononuclear Octahedral Dihalide  $\text{Mn}^{\text{II}}$  Complexes: An Investigation by Multi-frequency High-Field Electron Paramagnetic Resonance and Density Functional Theory. *Inorg. Chem.* **2007**, *46*, 4905–4916.
- (52) Duboc, C.; Ganyushin, D.; Sivalingam, K.; Collomb, M.-N.; Neese, F. Systematic Theoretical Study of the Zero-Field Splitting in Coordination Complexes of Mn(III). Density Functional Theory versus Multireference Wave Function Approaches. *J. Phys. Chem. A* **2010**, *114*, 10750–10758.
- (53) Bendix, J.; Brorson, M.; Schäffer, C. E. Accurate empirical spin orbit coupling parameters  $\zeta_{nd}$  for gaseous  $nd^d$  transition metal ions. The parametrical multiplet term model. *Inorg. Chem.* **1993**, *32*, 2838–2849.
- (54) Prins, R.; Biloen, P.; van Voorst, J. D. W. Electron Spin Resonance of Vanadocene. *J. Chem. Phys.* **1967**, *46*, 1216–1217.
- (55) Jackson, T. A.; Krzystek, J.; Ozarowski, A.; Wijeratne, G. B.; Wicker, B. F.; Mendiola, D. J.; Telser, J. Vanadocene *de Novo*: Spectroscopic and Computational Analysis of Bis( $\eta^5$ -cyclopentadienyl)vanadium(II). *Organometallics* **2012**, *31*, 8265–8274.
- (56) Jackson, T. A.; Krzystek, J.; Ozarowski, A.; Wijeratne, G. B.; Wicker, B. F.; Mendiola, D. J.; Telser, J. Addition to Vanadocene *de Novo*: Spectroscopic and Computational Analysis of Bis( $\eta^5$ -cyclopentadienyl)vanadium(II). *Organometallics* **2014**, *33*, 1325–1325.
- (57) La Mar, G. N.; Horrocks, W. D., Jr.; Holm, R. H. *NMR of Paramagnetic Molecules: Principles and Applications*; Academic Press, Inc.: New York, 1973.
- (58) Bertini, I.; Luchinat, C. Nuclear Magnetic Resonance of Paramagnetic Substances in Solution. In *Physical Methods for Chemists*, Drago, R. S., Ed.; Saunders College Publishing, 1992.
- (59) Bertini, I.; Luchinat, C.; Parigi, G. *Solution NMR of Paramagnetic Molecules: Applications to Metallobiomolecules and Models*; Elsevier Science BV: The Netherlands, 2001; Vol. 2.
- (60) Enders, M. Assigning and Understanding NMR Shifts of Paramagnetic Metal Complexes. In *Modeling of Molecular Properties*; Comba, P., Ed.; Wiley-VCH: Weinheim, Germany, 2011; pp 49–65.
- (61) Bertini, I.; Luchinat, C.; Parigi, G.; Ravera, E., Chapter 7 - Transition metal ions: shift and relaxation. In *NMR of Paramagnetic Molecules*, 2nd ed.; Bertini, I., Luchinat, C., Parigi, G., Ravera, E., Eds.; Elsevier: Boston, 2017; pp 175–253.
- (62) Kurland, R. J.; McGarvey, B. R. Isotropic NMR shifts in transition metal complexes: The calculation of the Fermi contact and pseudocontact terms. *J. Magn. Reson.* **1970**, *2*, 286–301.
- (63) Kruck, M.; Wadepohl, H.; Enders, M.; Gade, L. H. Giant Residual Dipolar  $^{13}\text{C}$ - $^1\text{H}$  Couplings in High-Spin Organoiron Complexes: Elucidation of Their Structures in Solution by  $^{13}\text{C}$ -NMR Spectroscopy. *Chem. - Eur. J.* **2013**, *19*, 1599–1606.
- (64) Plajer, A. J.; Colebatch, A. L.; Enders, M.; García-Romero, Á.; Bond, A. D.; García-Rodríguez, R.; Wright, D. S. The coordination chemistry of the neutral tris-2-pyridyl silicon ligand  $[\text{PhSi}(6\text{-Me-2-py})_3]$ . *Dalton Trans.* **2018**, *47*, 7036–7043.
- (65) Pavlov, A. A.; Savkina, S. A.; Belov, A. S.; Voloshin, Y. Z.; Nelyubina, Y. V.; Novikov, V. V. Very Large Magnetic Anisotropy of Cage Cobalt(II) Complexes with a Rigid Cholesteryl Substituent

from Paramagnetic NMR Spectroscopy. *ACS Omega* **2018**, *3*, 4941–4946.